RSC Advances

PAPER

View Article Online
View Journal | View Issue

Cite this: *RSC Adv.*, 2017, **7**, 30397

Transparent TiO_2 nanotubes on zirconia for biomedical applications

Sweetu B. Patel,[ad] Natalie Baker,[b] Isabella Marques,[b] Azhang Hamlekhan,[a] Mathew T. Mathew,[c] Christos Takoudis,[de] Craig Friedrich,[a] Cortino Sukotjo*[b] and Tolou Shokuhfar*[d]

Tissue discoloration in dental implant patients with thin gingival tissue is one of the many causes of dental implants' revision surgery. Therefore, the purpose of this study is to address this issue by developing a surface that has a "tooth like bright colored" appearance while at the same time enhancing the bone implant integration. A biomimetic surface is fabricated by forming transparent TiO_2 nanotubes on zirconia (TTNZ) that can enhance the proliferation and attachment of human mesenchymal stem cells (hMSCs) as compared to roughened ZrO_2. This surface treatment was aimed to resolve tissue discoloration and aesthetic appearance problems for dental implant patients, while also enhancing biocompatibility. TiO_2 nanotubes (TNTs) were formed using an electrochemical anodization technique in an electrolyte comprised of NH_4F, ethylene glycol and water. The presence of TNTs on the ZrO_2 substrate was detected by field emission scanning electron microscopy (FESEM). Optical images of longer anodized (20 and 30 min) samples show the white colored appearance characteristic of ZrO_2 and FESEM confirmed the presence of TNTs on anodized samples. Surface characteristics of all samples were analyzed using water contact angle analysis, Fourier-transform infrared spectroscopy, white light interferometry and FESEM. Quantitative and qualitative biocompatibility analysis of treated and non-treated ZrO_2 surfaces were obtained by performing FESEM, 3-(4,5-dimethylthiazol-2-yl)-2,5-diphenyl-2*H*-tetrazolium bromide (MTT) assay and fluorescence microscopy. FESEM revealed well-elongated and well-spread cell morphology on the nanotubular surface as compared to roughened ZrO_2. Additionally, MTT assay showed a significantly high cell proliferation for anodized Ti–ZrO_2 surface as compared to roughened ZrO_2 after 7 days of incubation.

Received 6th April 2017
Accepted 16th May 2017

DOI: 10.1039/c7ra03940a

rsc.li/rsc-advances

Introduction

Titanium (Ti) metal has been widely utilized for biomedical applications for decades due to its beneficial surface properties that allow such foreign implants to survive within the complex biological environment.[1] Additionally, according to American Academy of Implant Dentistry, 3 million population have dental implants with numbers increasing every year.[2] However, tissue discoloration around dental implant sites in patients with thin gingival tissue is of great concern, since it results in dental implant revision surgeries.[3,4] Therefore, much attention has been paid to resolve this shortcoming of titanium dental implants. ZrO_2 is a potential alternative for titanium due to its high flexural strength, fracture resilience, and similar chemical properties to that of titanium;[4–9] additionally, it is a ceramic of white colored appearance, which makes it a suitable material for patients with thin gingiva and metal ion sensitivity.

Various *in vivo* studies have been performed on understanding the tissue response surrounding ZrO_2 implants as compared to standard titanium implants. Depprich *et al.* investigated the effect of roughened ZrO_2 and Ti implants inside the tibia of minipigs in terms of their osseointegration property.[12] The histology and histomorphometric analysis concludes that there is no significant difference in cellular response between ZrO_2 or titanium implants.[12] Moreover, Gahlert *et al.* investigated the effect of roughened ZrO_2 *vs.* titanium implants inside the adult pigs by detecting peri-implant bone density and bone-implant contact ratio around the respective materials.[13] This study also supported Depprich *et al.*'s data on the similar bone-implant interaction of ZrO_2 in comparison with Ti implants.[12] On the other hand, Gahlert *et al.* investigated biomechanical fixation of implants constructed

[a]*Department of Mechanical Engineering-Engineering Mechanics, Michigan Technological University, Houghton, MI 49931, USA*

[b]*Department of Restorative Dentistry, University of Illinois at Chicago, Chicago, IL 60612, USA. E-mail: csukotjo@uic.edu*

[c]*Department of Biomedical Sciences, University of Illinois at Chicago, Rockford, IL 61101, USA*

[d]*Department of Bioengineering, University of Illinois at Chicago, Illinois 60607, USA. E-mail: tolou@uic.edu; Tel: +1 312 996 2335*

[e]*Department of Chemical Engineering, University of Illinois at Chicago, Illinois 60607, USA*

from machined ZrO_2, roughened ZrO_2 and roughened Ti after 4, 8 and 12 weeks through torque removal testing.[14] Significantly high removal torque values were obtained for roughened Ti implants followed by roughened ZrO_2 and machined ZrO_2.[14] This indicates that the biomechanical fixation of ZrO_2 implants is weak when compared to Ti. This suggests that further surface modification investigation is required for ZrO_2 based implants to improve their biomechanical fixation, bone density and bone-implant contact ratio. Even though the benefits of ZrO_2 are known, its ability to osseointegrate or create strong bone-implant contact remains somewhat uncertain; therefore, further study to enhance the success rate of ZrO_2 implants appear to be necessary.[10,11]

Previously, studies have also been performed to enhance the properties of ZrO_2 through surface modification including sandblasting, acid etching, anodization, and polymeric coating (*i.e.* poly(lactic acid) and poly(3/4-caprolactone)) *etc.*[14,15] In the study performed by Maeda *et al.* osteoblast activity was monitored on poly(lactic acid) coating and imogolite (aluminum silicate nanotubes) treated poly(lactic acid) coating. From the results, it was observed that the polymer treated with aluminum silicate nanotubes enhances the MC3T3-E1 adhesion on the surface. The reason for the increase in cellular bioactivity is reported as due to rougher surface texture that is obtained after treating with imogolite.[15] However, aluminum silicate poses the health risk of fibrosis if it detaches from the substrate, thereby interfering with bone-implant interaction, as reported by Elmore AR *et al.*[16] Additionally, Frandsen *et al.* investigated the effect of osteoblasts on TiO_2 nanotube coated ZrO_2 *vs.* bare ZrO_2. They also observed improved cell behavior on TiO_2 nanotube coated ZrO_2 compared to bare ZrO_2.[17] The main difference between their study and the present study is that (1) they used a sputtering technique to deposit titanium, whereas in our study an e-beam evaporation technique is used to deposit Ti, (2) they anodized Ti at 20 V for 15 min, which produces porous structure at low voltage, whereas in the present study, the Ti is anodized at 60 V for various times, producing tubular morphology as shown in FESEM images, (3) after anodization, in ref. 17, nanotubes were annealed to form anatase, whereas, no annealing was performed in our study and (4) in our study, white colored appearance of ZrO_2 substrate is observed in the presence of TiO_2 nanotubes on the surface.

It is well established that TiO_2 nanotubes (TNTs) enhance the implant's surface properties by providing nanoscale roughness for increased cellular adhesion thereby improving osseointegration compared to acid etched or sandblasted surfaces.[18–21] TNTs also improve the physiochemical characteristics of surfaces as shown through their ability to maintain surface wettability for a period of at least one month compared to smooth or rough Ti surfaces.[22–24] Hydrophilic surfaces attract more fibronectin (FN) and vitronectin (VN) protein from the body fluids, which are essential sites for cellular attachment and proliferation.[21,25,26] Additionally, TNTs have the capability to store drugs of interest such as BMP2, TGF-beta *etc.* for patients suffering from osteoporotic bone and being treated with growth factors to stimulate bone-ingrowth onto the implants.[27,28] These nanotubes may also act as a drug reservoir for anti-infection or anti-inflammatory drugs whose controlled and systematic release to the implant site may prevent complications due to post-surgery biological reactions.[29–32] To-date, these aforementioned benefits of TNTs have been introduced on CP-Ti or Ti-alloy surfaces. In this study, a hybrid surface is prepared with transparent TNTs on ZrO_2 substrates that possess white colored appearance, alleviate the possibility of metal ion allergic reactions, and provide benefits of nanotubular features.

The objectives of this study were to (1) fabricate surfaces with transparent titania nanotubes on zirconia substrates (TTNZ), (2) characterize their physiochemical and chemical surface characteristics with water contact angle analysis, Fourier transform infrared spectroscopy, white light interferometry, field emission scanning electron microscopy (FESEM) and optical appearance, and (3) investigate the biocompatibility of each surface using MTT assay, fluorescence microscopy and FESEM.

Methods and materials

Sample preparation

ZrO_2 discs of 15 mm diameter and 1 mm thickness were employed for the experiments. All discs were roughened by sandblasting with 50 μm Al_2O_3 particles (Trinity Tool Company, Fraser MI, USA) at 517 kPa for 10 s. Following this sandblasting procedure, all discs were cleaned by sequential sonication in ethanol and de-ionized (DI) water for 15 min. Cleaned ZrO_2 discs were then coated with a 500 nm thick titanium film using e-beam evaporation employed at Nanotechnology Core Facility (NCF) at University of Illinois at Chicago (UIC). Ti deposited ZrO_2 samples are designated as Ti–ZrO_2. The base pressure of reactor was maintained at 5×10^{-7} Torr with a rotating sample holder to obtain even film growth. Titanium evaporation current was maintained at 47 mA and the voltage was 10 V. The growth rate of titanium on ZrO_2 was measured to be $\sim$1 Å s^{-1}. Ti–ZrO_2 samples were then anodized using an electrochemical anodization technique, where Ti–ZrO_2 was the working electrode (WE) and graphite was the counter electrode (CE). Electrodes were connected to the voltage source (Keithley 2400 SourceMeter, Cleveland, OH, USA), which supplied a constant voltage of 60 V for 10, 20 and 30 min. The anodization electrolyte was comprised of 2 vol% H_2O and 0.25 wt% NH_4F (Sigma-Aldrich, St. Louis, MO, USA) in ethylene glycol (Fisher Scientific, Pittsburgh, PA, USA) and it was continuously stirred with a magnetic stirrer to maintain a homogeneous environment throughout anodization. A total of four groups were investigated in this study: roughened ZrO_2, 10TNZ (10 min anodized sample with TiO_2 nanotube coated ZrO_2), 20TTNZ (20 min anodized samples with transparent TiO_2 nanotubes coated zirconia), and 30TTNZ (30 min anodized samples with transparent TiO_2 nanotubes coated zirconia).

Surface characterizations

Field emission scanning electron microscopy (FESEM, JSM-6320F, JEOL, Musashino 3-chome Akishima Tokyo, Japan) was used to analyze the external surface morphology of roughened ZrO_2, 10TNZ, 20TTNZ and 30TTNZ samples. The sample of

interest was mounted on an aluminum stub with the help of double sided conductive carbon tape for imaging. FESEM images were obtained with acceleration voltages of 3.8 kV, and specimens were observed with magnifications of 10 000× and 50 000×. White light interferometry (WLI, NewView 6300, Zygo Corporation, Middlefield, Connecticut, USA) in Tribology Lab at Rush University Medical Center was used to measure surface roughness of ZrO_2, and anodized Ti–ZrO_2 samples. Transparency of the anodized samples were observed by holding the samples against white light where the top surface of the samples faced the light and the optical image was captured from the back side, as shown in graphical abstract. This allows the light to pass through if the sample is transparent and no light passes through if the sample is non-transparent. Diffuse reflectance Fourier-transform infrared spectrometry (FTIR, Nicolet, Madison, WI, USA) was used to probe the surface composition of ZrO_2 and anodized Ti–ZrO_2 samples. ZrO_2 was used as a background for ZrO_2 sample scans; moreover, non-anodized Ti–ZrO_2 was used as a background for anodized Ti–ZrO_2 sample scans. Before running the FTIRS experiment, each sample was kept inside the FTIRS chamber for 1 h in order to stabilize the internal conditions and optimize the signal to noise ratio. FTIRS spectra were obtained with 2 cm^{-1} resolution and 512 scans over the wavenumber range of 400–4000 cm^{-1}. Qualitative analysis by de-convoluting FTIR spectra was performed using spectral peak-fitting software with a linear background and Gaussian–Lorentian peak shape function.

Surface wettability

Water contact angle (WCA) measurements were obtained using a sessile drop method with the help of Goniometer (Rame'-Hart NRL, Succasunna, NJ, USA) to determine the surface hydrophilicity. During WCA measurements, 5 μL of DI-water was placed on the respective surfaces followed by image capturing. The WCA on each surface was analyzed using Image-J Analysis software. The wettability of all samples was monitored after 0, 1, 2, 3 and 6 days and thereafter every 7 days for a period of 1 month. Before measuring WCA on day 0, all the samples were first cleaned with methanol for 10 min followed by a DI water wash for 10 min. For the rest of the measurements over a period of one month, each sample was merely cleaned by blow-drying with N_2 gas (Grade 4.8, 99.998%, NIZ300 Progressive Industries Inc., Sylacauga, Al, USA) before performing WCA. After WCA measurements, samples were stored in a plastic Petri dish until the next measurement.

In vitro cell viability tests

Human Mesenchymal Stem Cells (hMSCs) (derived from adult bone marrow, provided by Tulane University) were used for cell viability tests on each surface. Prior to culturing cells on different substrates, hMSCs were made ~80–90% confluent in a cell culture media composed of Dulbecco's modified Eagle medium (DMEM; Hyclone, GE Healthcare Life Sciences, PA, USA) supplemented with 10% fetal bovine serum (FBS; Gibco by Life Technologies, NY, USA) and 1% penicillin and streptomycin (Gibco by Life Technologies, NY, USA). The incubator environment was kept at 37 °C and 5% CO_2. After cells reached 80–90% confluence, they were trypsinized (Hyclone, GE Healthcare Life Sciences, PA, USA) to detach them, and then centrifuged at 1200 rpm for 5 min. The supernatant fluid was discarded and cells were washed twice with phosphate buffer saline (PBS, Gibco by Life Technologies, NY, USA). Then the cells were re-suspended in culture media to obtain healthy cells for culturing. All samples were first sterilized in 70% ethanol. After sterilizing the samples, 2×10^4 cells were cultured on each substrate. The samples seeded with cells were incubated at 37 °C and 5% CO_2 environment.

MTT assay. Cell viability was detected by measuring the absorbance using the MTT assay after 1 and 6 days of incubation in 37 °C and 5% CO_2. First, 3-(4,5-dimethylthiazol-2-yl)-2,5-diphenyl-2*H*-tetrazolium bromide (MTT, Sigma Aldrich, St. Louis, MO, USA) was diluted in PBS with a concentration of 0.5 mg of MTT l^{-1} of solution. After preparing the MTT solution, culture media and MTT solution were mixed in 1 : 1 v/v ratio. First, the cells were washed with PBS twice. Then 500 μl of mixed MTT and culture media solution was added to the cells on the discs. The cells were again incubated for 4 h. Then 500 μl of dimethyl sulfoxide (DMSO, Fisher Scientific, Pittsburgh, PA, USA) was added to each well. Then again the cells were incubated for 24 h. The absorbance signal was measured using a fluorescence reader (SpectraMax Plus, Molecular Devices, Sunnyvale, CA, USA) with 570 nm and 600 nm wavelengths.

Fluorescence microscopy. Cell spreading morphology was observed after 3 and 24 h of seeding. Prior to fluorescence microscopy, cells were fixed with 3.7% formaldehyde in PBS for 15 min at room temperature. Cells were stained using ActinRed 555 Readyprobe (Molecular Probes by Life Technologies, Grand Island, NY, USA) for 30 min, NucBlue (Molecular Probes by Life Technologies, Grand Island, NY, USA) for 20 min, and 0.1% Triton X-100 for 15 min to probe the nucleus and actin filaments of the cells.

FESEM. Cell morphology was observed after 6 days. Prior to FESEM, cells were fixed with 3.7% formaldehyde (Fisher Scientific, Pittsburgh, PA, USA) in PBS for 15 min at room temperature. The cells were then rinsed with PBS for 15 min four times. Then the cells were dehydrated in increasing concentration of ethanol at 25, 50, 75, 90 and 100% for 10 min once except for 100% ethanol dehydration, which was performed twice. Prior to FESEM imaging, samples fixed with cells were sputter coated with ~5–7 nm Au/Pd coating. FESEM images were obtained with acceleration voltages of 10 kV, and specimen with 2000 magnifications.

Statistical analysis

SPSS software (SPSS v. 20.0, SPSS Inc., Chicago, IL, USA) was used to perform statistical analysis. One-way ANOVA was used to determine the statistical difference in surface roughness and wettability before and after anodization, and the dimensions of the nanotubes upon different anodization times. Tukey Honest Significant Difference (HSD) *post hoc* analysis was used for pairwise comparison within and between each group. For all the

analysis, p-values <0.05 were considered as statistically significant.

Results and discussion

Current–time behavior

Formation of TiO_2 nanotubes on Ti through electrochemical anodization process is divided into three stages: (i) field assisted oxidation, where Ti oxidizes to TiO_2, (ii) field assisted dissolution, where nucleation of pore formation is initiated and (iii) equilibrium between field assisted oxidation and dissolution, where formation and dissolution of TiO_2 takes place at a constant rate.[30–32] Fig. 1 shows the current–time transient curve of Ti–ZrO_2 samples during anodization for the first 10 min. Such a graph allows extrapolating the information related to the chemical reaction on the surface that leads to the formation of well-aligned nanotubular structures.

The current–time curve of Ti–ZrO_2 shows three stages. In stage 1, a drastic drop in the current is observed. This significant current drop is due to the formation of a barrier TiO_2 layer on the Ti surface when 60 V is applied. Initially, mass evolution of H_2 gas is observed near the cathode (graphite) due to the high electron conductivity.[31] This H_2 gas evolution arises from the dissociation of H_2O from electrolyte that releases H^+ ions along with OH^- and O^{2-} ions. H^+ ions combine to form H_2 at the cathode, whereas, negatively charged ions (*i.e.* OH^- and O^{2-}) migrate towards the anode (Ti–ZrO_2) and diffuse to the Ti/TiO_2 interface, where they react with Ti^{4+} ions and form TiO_2 and/or $Ti(OH)_4$.[21,33,34] Consequently, the oxidation process of stage I is dominated on the surface initially. In stage II, the current profile is observed to steadily decrease indicating lessening of oxidation, with stabilizing of the current likely due to limitation in electron conductivity;[31,33] simultaneously, this stabilization may also be resulted from the nucleation of pore formation on the surface, which explains the initiation of ionic conductivity on the surface (TiO_2/electrolyte interface).[31] The generation of pores increases the surface area of Ti–ZrO_2 that facilitates the diffusion of ionic species (*i.e.* O^{2-}, OH^-, Ti^{4+}, or F^-) into/from the anode in comparatively large amounts, thereby decreasing the resistance of the film.[31,34] During stage II, F^- ions from ammonium fluoride, react with TiO_2 and $Ti(OH)_4$ to form TiF_6^{2-}, which is soluble in electrolyte, thereby forming pores and well organized nanotubes.[33,34] Finally, in stage III, a further decrease and stabilization of the current is observed. During this phase, the rate of TiO_2 formation at the Ti/TiO_2 interface and the rate of TiO_2 dissolution at the TNTs pore bottom is in equilibrium. Because there is limited amount of Ti (500 nm-thick) on the ZrO_2 substrate, once the titanium layer has fully oxidized, the dissolution reaction would be the leading reaction. In addition, although dissolution is the leading reaction, current will not increase because the underlying substrate of titanium is ZrO_2 ceramic that resists ionic and electronic conduction. Due to these reasons, transparent nanotubes are obtained at longer anodization duration (20 and 30 min) as shown in Fig. 2.

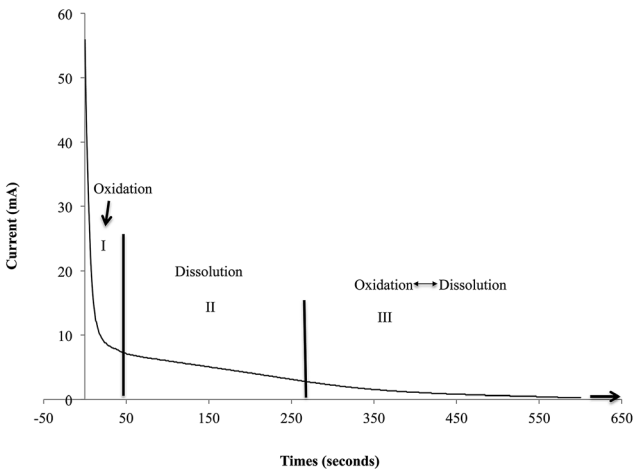

Fig. 1 Current–time transient analysis of Ti–ZrO_2 sample in an electrolyte composed of ammonium fluoride, ethylene glycol, and water at 60 V. This figure shows the current profile during the anodization process. In region I, a drastic drop in current is observed, which is due to the oxidation of Ti. In region II, the current stabilizes, which is due to the dissolution of TiO_2 and limitation in O^{2-} diffusion through the barrier layer. In region III, the rate of ionic exchange decreases even further, which is due to the equilibrium between oxidation and dissolution and having ZrO_2 ceramic as the substrate, which further prevents ionic exchange.

Field emission scanning electron microscopy (FESEM)

Fig. 2 shows the FESEM images of ZrO_2 and anodized Ti–ZrO_2 samples. Fig. 2a shows the surface morphology of untreated ZrO_2 sample. It is observed that the surface possesses irregular roughness, which is from the sandblasting procedure. The upper inset on Fig. 2a shows the optical visualization of ZrO_2 samples, which displays a bright "tooth-color" appearance. Fig. 2b shows the surface of e-beam evaporation deposited titanium on ZrO_2 substrates (Ti–ZrO_2) post 10 min of electrochemical treatment. The surface topography of 10 min anodized Ti–ZrO_2 samples (10TNZ) shows that nanotubes with 26.8 ± 4.5 nm diameter are observed evenly throughout the surface with length 0.63 ± 0.03 μm (as shown in upper left inset, Fig. 2b). The optical image of 10 min anodized samples display similar gray colored appearance similar to non-anodized Ti region. This gray colored appearance of 10TNZ samples likely arises from a non-anodized titanium layer between the top TNT layer and bottom ZrO_2 substrate. When anodization duration is 10 min, only some titanium might have been anodized to form TiO_2 nanotubes (TNTs) leaving a layer of non-anodized Ti, thereby providing a surface with three layers (TNT layer, non-anodized Ti, and ZrO_2 substrate), imparting an unfavorable gray colored appearance of Ti. This indicates that at low anodization duration (10 min), non-transparent nanotubes are obtained (schematic representation in graphical abstract).

Similarly, Fig. 2c and d show the surface topography and cross section of 20 (20TTNZ) and 30 (30TTNZ) min anodized Ti–ZrO_2 samples, respectively. Compared to 10TNZ samples, the density of the pores on 20TTNZ and 30TTNZ samples has decreased. This is due to the widening of the pore diameter from 26.8 ± 4.5 nm (10TNZ) to 35.3 ± 6.9 nm (20TTNZ) and 36.3

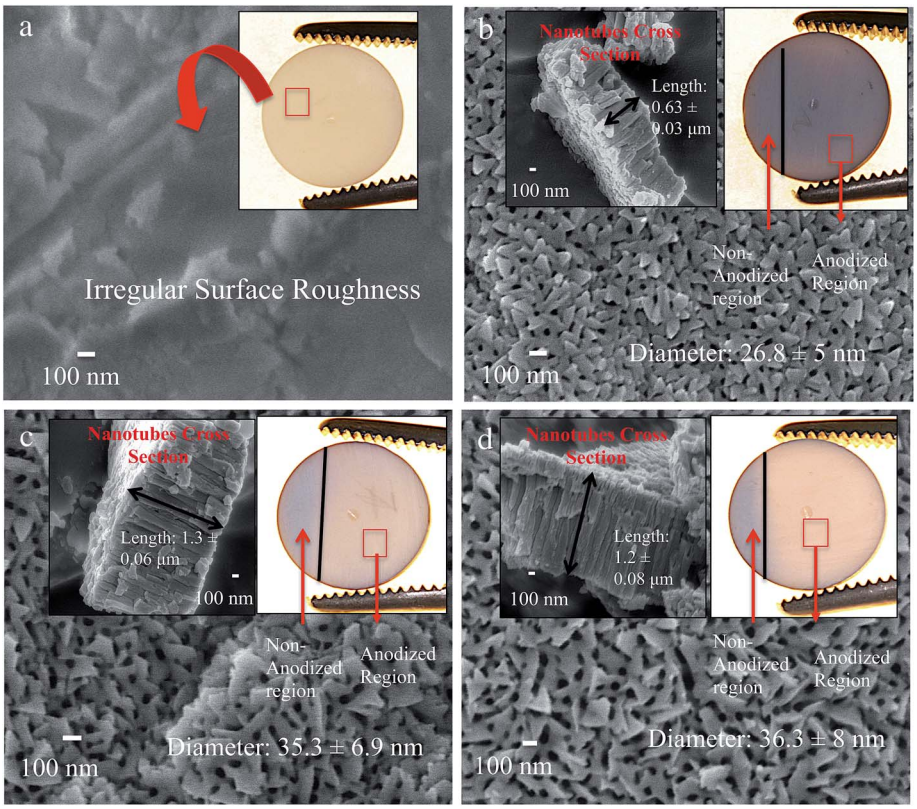

Fig. 2 FESEM images for (a) ZrO_2, (b) 10 min anodized Ti–ZrO_2, (c) 20 minute anodized Ti–ZrO_2, and (d) 30 min anodized Ti–ZrO_2. Right upper insets show the optical appearance of each sample before and after electrochemical treatment and the cross section shown left displays the length of TiO_2 nanotubes. Anodization was performed in 2 vol% H_2O, 0.25 wt% NH_4F and EG.

± 8 nm (30TTNZ). According to Tukey HSD *post hoc* analysis, an increase in diameter between 10 and 20 or 30 min anodized surface is significant as concluded by $p < 0.05$. Additionally, a significant increase in length was observed for 20TTNZ (1.3 ± 0.06 μm) and 30TTNZ (1.2 ± 0.08 μm) (Tukey HSD *post hoc* analysis with $p < 0.05$), as compared to 10TNZ samples (0.63 ± 0.03 μm), which is shown in Fig. 2c and d. This increase in length of TNTs, when anodization duration increases to 20 and 30 min, is due to the presence of non-anodized Ti layer after 10 min anodization, which can further oxidize and dissolve to form nanotubes. When the anodization duration is increased to 20 and 30 min, longer nanotubes are obtained of the order of 1 μm. On the other hand, no significant difference was observed in TNTs length when anodization duration was increased from 20 to 30 min (Tukey HSD *post hoc* analysis $p > 0.05$). This stabilization in the growth of nanotubes length after 20 min is likely due to the complete anodization of 500 nm deposited Ti within 20 min, which leaves no Ti for further oxidation and dissolution process on extension to 30 min.

Additionally, the length of the nanotubes is observed to be higher (~1.3 μm for 20 and 30 min anodization) than the thickness of deposited titanium (500 nm-thick). There are two factors affecting the expansion of the film: (1) Pilling–Bedworth ratio and (2) flow model mechanism of the nanotubes formation. The Pilling–Bedworth ratio (PBR) is the metal expansion factor when it is converted into an oxide.[33] This means that when titanium is exposed to the oxygen source, titanium splits into Ti^{4+} and $4e^-$ ions, which then react with O^{2-} to form TiO_2.[34] As the oxide thickness increases, the Ti^{4+} ions diffuse towards the surface and O^{2-} diffuse towards the metal/oxide interface. This oxidation process introduces a volume expansion to the metal.[35,36] Such volume ratio of oxide to metal is the PBR factor.[35,36] The PBR of amorphous TiO_2 has been reported to be 2.43, which is the ratio of amorphous TiO_2 to Ti metal.[33] Additionally, according to the flow mechanism of nanotubes formation, when the voltage is applied to the titanium, the strong electric field across the oxide layer induces stress in the barrier layer due to volume expansion caused by ion movements within the oxide layer. Such volume expansion and ionic transport exerts compressive stress along the tubular oxide interface due to the high electric field zone in the nanotubes, thereby facilitating the plastic flow/movement of barrier oxide towards the walls of the nanotubes.[30,36,37]

Optical images of 20TTNZ (Fig. 2c) and 30TTNZ (Fig. 2d) samples show that a transparent nanotubular layer is obtained when anodization is performed for 20 and 30 min. The anodized region of 20TTNZ and 30TTNZ show similar optical appearance to that of ZrO_2 samples, unlike 10TNZ samples. This suggests that when Ti–ZrO_2 samples were anodized for longer duration (20 and 30 min), all deposited Ti might have anodized completely, thereby providing the surface with two layers (transparent TiO_2 nanotubes layer and ZrO_2 layer)

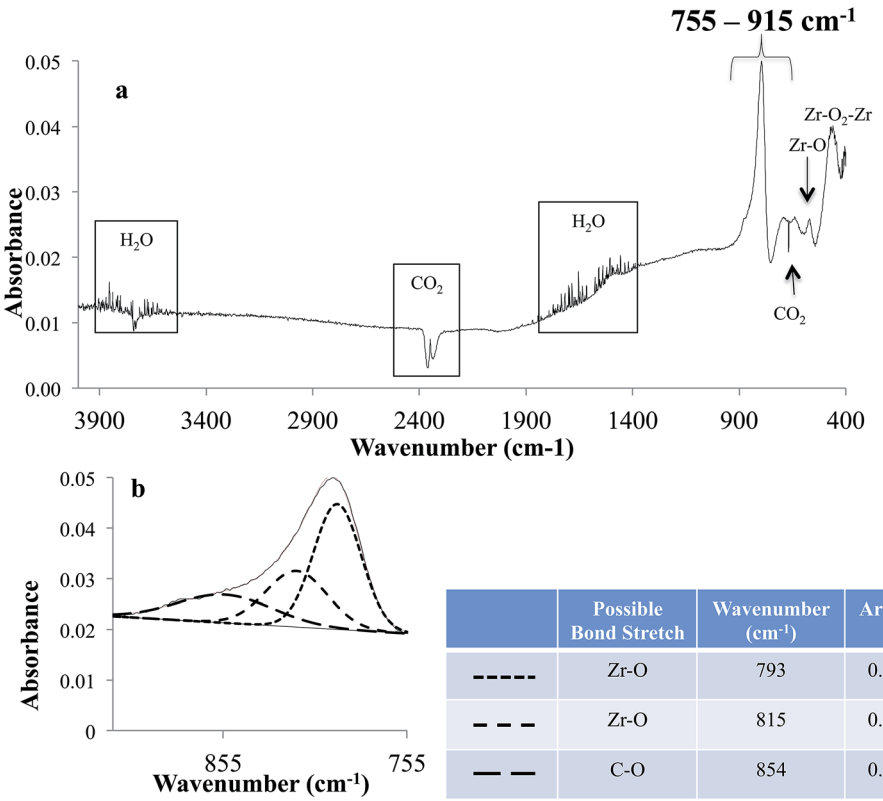

	Possible Bond Stretch	Wavenumber (cm^{-1})	Area
-----	Zr-O	793	0.8
– – –	Zr-O	815	0.5
— —	C-O	854	0.4

Fig. 3 FTIR spectra of the ZrO_2 sample: (a) whole spectrum (4000–400 cm^{-1}) and (b) de-convolution of the region (755–915 cm^{-1}). The legend in (b) provides the possible bond stretch assignments, peak position and area under the curves.

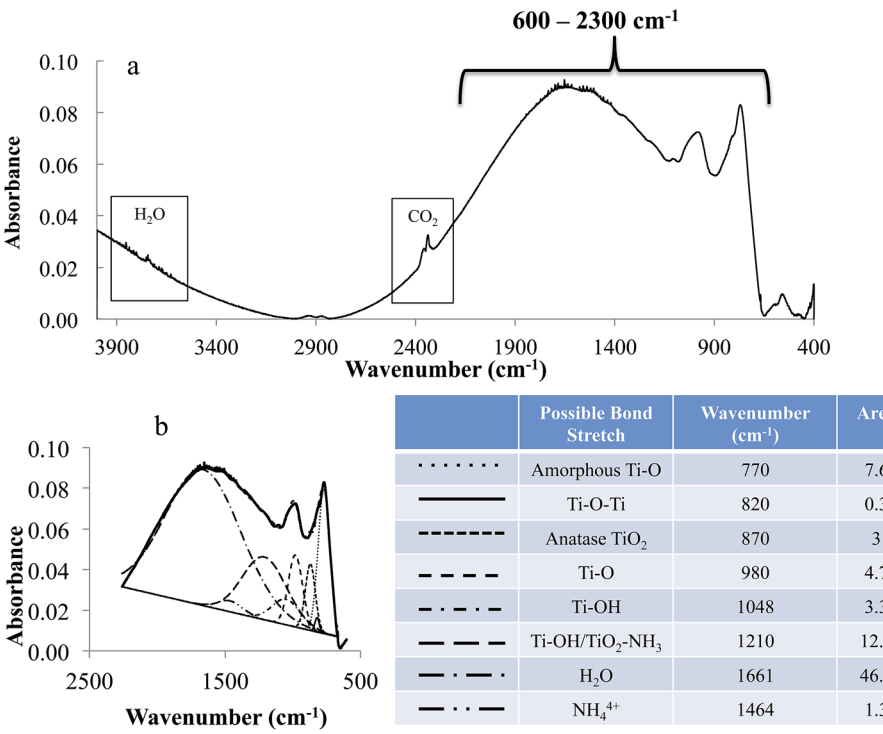

	Possible Bond Stretch	Wavenumber (cm^{-1})	Area
·····	Amorphous Ti-O	770	7.6
———	Ti-O-Ti	820	0.3
-------	Anatase TiO_2	870	3
– – – –	Ti-O	980	4.7
– · – · –	Ti-OH	1048	3.3
— — —	Ti-OH/TiO_2-NH_3	1210	12.5
— · — ·	H_2O	1661	46.6
— · · —	NH_4^{4+}	1464	1.3

Fig. 4 FTIR spectrum of anodized Ti–ZrO_2 samples. (a) Whole spectrum (4000–400 cm^{-1}) and (b) de-convolution of the region (600–2300 cm^{-1}) from anodized Ti–ZrO_2 samples. Legend in (b) provides the possible bonds stretch, peak position and area under the curves. Anodization condition is same as mentioned in Fig. 2.

Table 1 Quantitative comparison of average surface roughness and root mean square of the samples with different treatments; a: $p < 0.05$ compared to b and c; b: $p < 0.05$ compared to c

Surface topography	Average roughness (R_a)/μm	Root mean square (rms)/μm
ZrO_2	0.71 ± 0.13^a	0.91 ± 0.16^a
10 min anod. Ti–ZrO_2	0.84 ± 0.04^b	1.04 ± 0.05^b
20 min anod. Ti–ZrO_2	1.26 ± 0.04^c	1.46 ± 0.09^c
30 min anod. Ti–ZrO_2	1.18 ± 0.04^c	1.42 ± 0.06^c

imparting a bright colored appearance characteristic of ZrO_2. Such transparent appearance of substrate when complete anodization occurs was also observed in previous studies, however, their substrate was ITO instead of ZrO_2.[38–40] TNT decorated implants have shown many potential benefits for implants; however, over time, the quality of patients' life is affected due to the tissue discoloration in patients with thin gingival tissues and metal allergic reactions. In this study, from FESEM and optical imaging, it is observed that decorating ZrO_2 substrates (light colored ceramic) with TNTs provides a novel bio-implant surface that provides all the benefits of TNTs. It is light in color compared to titanium implants, and it can prevent tissue discoloration in patients with thin gingival tissue and reduces allergic reaction to metals. In order to obtain high resolution cross-section of the nanotubes, further studies are required using a focused ion beam to obtain high-resolution TEM images of nanotubes on the Ti–ZrO_2 samples.

Fourier transform infrared spectroscopy

FTIRS data of the ZrO_2 sample is shown in Fig. 3. In the spectrum, the absorption peaks are observed for gas phase CO_2 at 2200–2400 and 667 cm^{-1} and H_2O in the ranges of 3600–3800 and 1400–1900 cm^{-1}, which are from the residual air of FTIR purging chamber. Additionally, absorption peaks featured at the lower wavenumber of 560 and 450 cm^{-1} are due to Zr–O and Zr–O_2–Zr vibrational stretch, respectively.[41,42] Fig. 3b shows the de-convoluted spectrum of the intense peak observed in the region 755–915 cm^{-1}. This region is the superposition of various absorption bands including Zr–O at 793 and 815 cm^{-1} and C–O at 854 cm^{-1}, respectively.[43–45] Absorption peaks for C–O is likely from carbon dioxide adsorbed on to ZrO_2.[46] Fig. 4 shows the FTIRS spectrum of anodized Ti–ZrO_2 samples. An absorption peak around 535 cm^{-1} is observed, which is the apparent feature of a Ti–O bond stretch.[47–49] Additionally, superposition of multiple peaks in the region 600–2300 cm^{-1} is also observed, which is de-convoluted in Fig. 4b. Previously, it has been concluded that anodizing titanium in ammonium fluoride and ethylene glycol electrolyte forms nanotubes with surface composition of TiO_2 and $Ti(OH)_4$.[19,21] Therefore, the features in the region 600–2300 cm^{-1} for the anodized sample are likely arising due to the presence of Ti–O at 980 and 770 cm^{-1} from surface vibrations, Ti–O–Ti stretch at 820 cm^{-1}, and Ti–OH at 1210 cm^{-1}.[48,50–52] There is also likelihood for the presence of anatase TiO_2 at 870 cm^{-1}, which has been observed previously under similar anodization parameters and conditions at 60 V.[19,21,50] Some features of NH_4^+ at 1464 cm^{-1}, and Ti–N at 1075 cm^{-1} are also observed, which are from remnants of electrolyte.[19,53,54]

It is likely that the de-convolution may include some deviation in the peak positions from literature values of the absorption bands due to (i) uncertainties from the sloped baseline due to irregular surface roughness, and (ii) absorption shift for a particular bond stretch due to the effect of other chemicals/

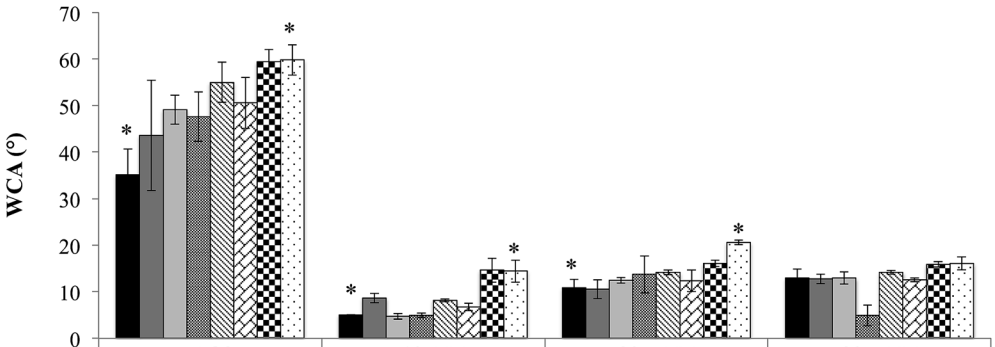

	ZrO2	10TNZ	20TTNZ	30TTNZ
Day 0	35.1	5	10.8	12.9
Day 1	43.6	8.6	10.5	12.7
Day 2	49.1	4.7	12.4	12.9
Day 3	47.6	4.9	13.7	4.9
Day 6	55	8.1	14.1	14.1
Day 13	50.6	6.7	12.3	12.5
Day 20	59.4	14.6	16.1	15.9
Day 27	59.8	14.4	20.6	16.1

Fig. 5 Surface wettability of ZrO_2, 10TNZ, 20TTNZ and 30TTNZ samples over a period of one month. Wettability was measured every day for first three days followed by once every week over a period of one month. (*) Indicates a statistical significance within groups with $p < 0.05$.

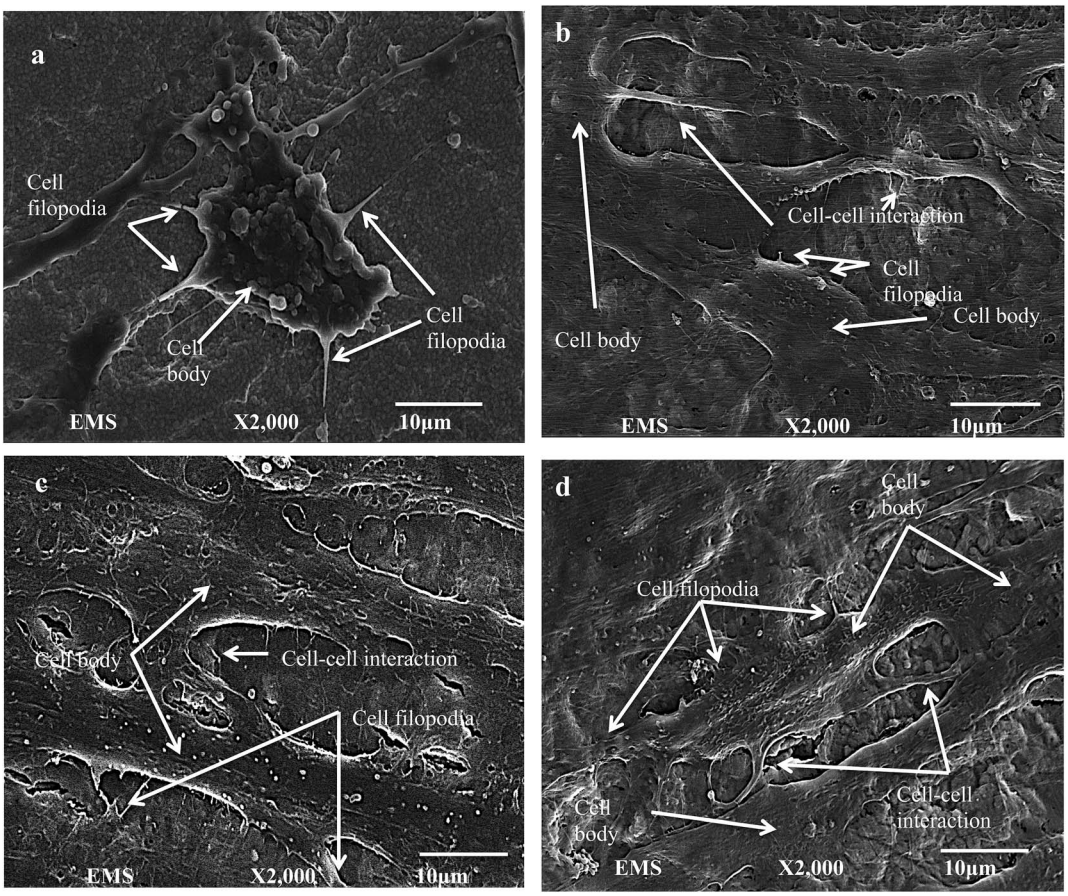

Fig. 6 FESEM images of hMSCs cells after 6 days of cell seeding on (a) ZrO_2, (b) 10TNZ, (c) 20TTNZ and (d) 30TTNZ. Cell body, filopodia, and cell–cell interaction are labeled with arrows.

molecular species present in the vicinity. Thus, study with controlled parameters is required to optimize the deconvolution of FTIRS data.

White light interferometry

White-light interferometry (WLI) was employed to probe the changes in surface roughness after each surface treatment on ZrO_2 substrate. The average surface roughness and root mean square of the samples are shown in Table 1. A significant increase in surface roughness is observed after anodization compared to roughened ZrO_2 samples. This is due to the increase in surface area owing to the formation of nanotubes on the Ti–ZrO_2 substrate; additionally, a further increase in surface roughness is observed after 20 and 30 min of anodization compared to the samples anodized for 10 min ($p < 0.05$; Tukey HSD *post hoc* analysis). This increase in surface roughness is likely due to the increase in length and diameter of the nanotubes compared to 10TNZ samples. FESEM images of the samples corroborate the surface roughness results, which shows that TNTs length and diameter increases when anodization duration increases. Finally, the surface roughness of 20 and 30 min anodized samples show no statistically significant difference, which is corroborated by the FESEM results (shown in Fig. 2c and d). This similar length nanotubes for 20 and 30 min anodization is due to the limited availability of the titanium layer on ZrO_2. Due to this limited titanium thickness, lengthening of the TNTs are hindered by the ZrO_2 substrates; therefore, nanotubes length remains stable when anodization duration was increased from 20 to 30 min. Upon further increase in anodization duration to greater than 30 min, there is a possibility of shortening of nanotubes, as the etching of nanotubes walls will dominate over oxidation due to the ceramic substrate. This behavior is not investigated in this study.

Water contact angle

Water contact angle (WCA) of ZrO_2, and 10, 20 and 30 min anodized Ti–ZrO_2 samples were monitored over a period of one month. Hydrophilic surfaces enhance osteoconduction, which improves the bone formation at the interface.[55] High surface wettability is required for improved fibronectin and vitronectin adsorption on the surface that makes focal complexes, which allows cells to make strong actin mediated anchorage with the implant, thereby improving bone-implant contact.[22,56,57]

Fig. 5 shows the WCA results of each surface over a period of 27 days. WCA of ZrO_2 samples on day 0 was hydrophobic compared to all other surfaces with WCA of $35.1 \pm 5.6°$, which increases to $59.8 \pm 3.2°$ by day 27. Such WCA of ZrO_2 is

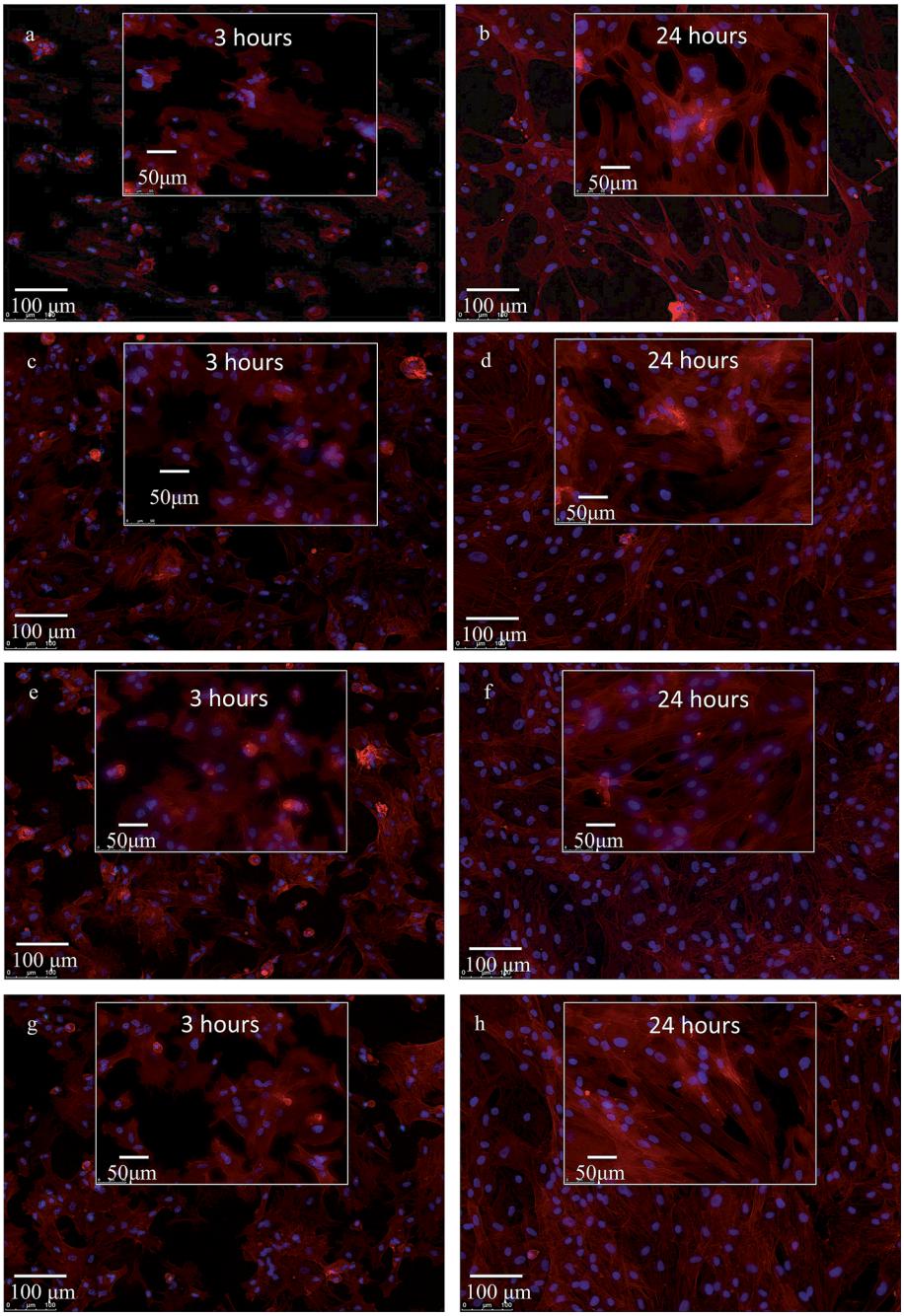

Fig. 7 Fluorescence microscopy of hMSCs cells on ZrO_2 (a and b), 10TNZ (c and d), 20TTNZ (e and f), and 30TTNZ (g and h) after 3 and 24 hours, respectively. Blue = nucleus; red = cytoskeleton.

corroborated by González-Martín *et al.*[58] Their study focused on investigating the surface free energy and wettability of zirconia based ceramics, which shows that the WCA of 5% yttria stabilized ZrO_2 is about 72°.[58] Akio Noro *et al.* also reported an increase in WCA of sandblasted ZrO_2 samples to ~80° after 21 days.[59] This increase in WCA over time when samples are stored in air is due to carbon contamination from the environment, as shown by the X-ray photoelectron spectroscopy data with carbon content increasing from ~20% (day 0) to ~45% (day 21).[59] After anodizing Ti on ZrO_2, the surface becomes super-hydrophilic with WCA of <5°, 10.8 ± 1.8°, and 12.9 ± 1.9° for 10TNZ, 20TTNZ, and 30TTNZ, respectively. For day 0, the difference in surface wettability between 10TNZ and 20TTNZ or 30TTNZ samples is likely due to the difference in surface roughness. There is a decrease in wettability for 10TNZ (14.4 ± 2.4°) and 20TTNZ (20.6 ± 0.5°) samples by day 27 compared to their day 0 wettability; moreover, a non-significant decrease was observed for 30TTNZ samples with WCA of 16.1 ± 1.4°. This decrease in surface wettability for 10TNZ and 20TTNZ samples may likely be due to the carbon contamination during the aging

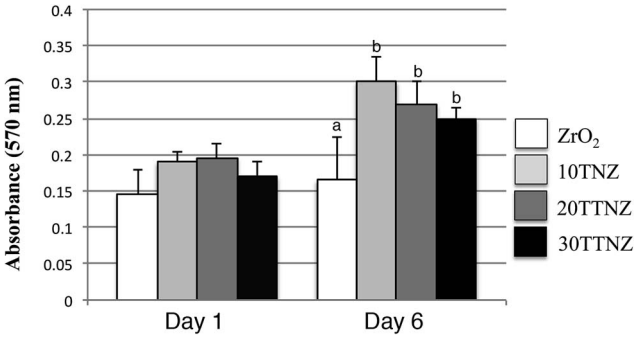

Fig. 8 Cell viability test on ZrO_2, 10TNZ, 20TTNZ and 30TTNZ (anodization conditions are indicated in Fig. 1) after 1 and 6 days of incubation in 5% CO_2 and 37 °C. (a) $p < 0.05$ compared to group (b).

period. However, compared to ZrO_2, anodized Ti–ZrO_2 samples are able to maintain their surface wettability to less than or about 20° over a period of 27 days. This anti-aging hydrophilic property of anodized titanium surface has been corroborated by our previous studies as well as in the literature.[22–24] The ability of an anodized surface to maintain their surface wettability has been extensively discussed previously by Shin *et al.*[21] They showed that when titanium is anodized in an electrolyte composed of EG, NH_4F and water, the composition of nanotube walls is $Ti(OH)_4$ and TiO_2 that has the ability to attract more water molecules making the surface hydrophilic.[21] The composition of nanotubes wall of $Ti(OH)_4$ and TiO_2 is also corroborated by the FTIR results, which was provided in the previous section.

The anti-aging property of TNTs is due to the surface composition of the nanotube walls, which contains $Ti(OH)_4$ that has a higher affinity for water than for contaminants.[19] Additionally, higher surface roughness of anodized Ti–ZrO_2 along with $Ti(OH)_4$ content, further improves its wettability, which can be explained by the Wenzel model. In the Wenzel model, if the WCA is between $0 < \theta < 90°$, then the higher the surface roughness, the higher the wettability.[61]

WCA of 10, 20 and 30 min anodized samples on day 0 shows that, 10TNZ samples were more hydrophilic with WCA of <5° compared to 20TTNZ and 30TTNZ with WCA of 10.8 ± 1.8° and 12.9 ± 1.9°, respectively. This difference in surface wettability between 10TNZ and 20TTNZ or 30TTNZ samples is likely due to the difference in surface roughness and presence of $Ti(OH)_4$. WLI results show that the average surface roughness of 10TNZ samples is significantly smaller ($p < 0.05$: Tukey *post hoc* analysis) compared to 20TTNZ and 30TTNZ samples. Therefore, high initial WCA of 20 and 30 min anodized samples may be due to the higher probability of air entrapment inside the nanotubes in addition to lower $Ti(OH)_4$ amount in TNTs walls due to conversion of $Ti(OH)_4$ to TiO_2 by condensation reaction of the hydrated oxide layer as the anodization duration increases.[19,30] Dahotre *et al.* explain this higher WCA behavior of rougher samples using the Cassie and Baxter model.[63] In their study, micro-textures of different roughness are created on Ti–6Al–4V alloy using laser-based optical interference and direct melting technique. They show that as the height of the grooves increases from 68.08 ± 0.02 nm to 208.08 ± 0.08 nm their WCA also increases from 70.7 ± 0.3° to 78.55 ± 0.45°. An increased volume of trapped air explains such increase in WCA on grooves with larger height compared to smaller height.[63]

Cell spreading, attachment and proliferation

Cell adhesion to the substrate is one of the determining factors for satisfactory bone–implant integration and cellular differentiation. After the initial cell attachment, they release extracellular matrix components which are collagenous and non-collagenous proteins. These proteins act as a scaffold for mineralization (calcium phosphate deposition) and thereby enhance bone formation and maturation.[64–67] Higher cell spreading and attachment is essential for cell differentiation at the bone–implant interface. Studies have shown that when cells elongate, their cytoskeleton reorganizes and leads to changes in the conformation of nucleus, which triggers the cell differentiation process through DNA unfolding.[68] Fig. 6 shows FESEM images of the cell shape and attachment morphology on each surface. Fig. 6a show the FESEM image of cells on roughened ZrO_2 samples. Rounded cell morphology with many filopodia anchoring the surface is observed along with cell–cell interaction through filopodia. Similar cell bioactivity was observed on ZrO_2 in the study performed by Depprich *et al.*[12] They investigated the bone-to-implant contact after 1, 4, and 12 weeks of ZrO_2 and titanium implants inside minipigs. Histological data showed that the bone-to-implant contact after 1 week on titanium was 47.3% ± 9.1 and for zirconia was 35.3% ± 10.8, which was not statistically significantly different (similar behavior was seen for weeks 4 and 12).[12] Similarly, Pae *et al.* investigated the human gingival fibroblast (HGF) attachment on Ti and ZrO_2 substrates. In their study, the degree of cell proliferation was measured after 24 and 48 h.[69] They too found a non-statistical significant difference in HGF proliferation between Ti and ZrO_2 samples.[69]

On the other hand, well-elongated and well spread cells with filopodia and cell–cell interactions are observed on anodized Ti–ZrO_2 samples compared to roughened ZrO_2 samples as shown in Fig. 6b–d. Popat *et al.* observed similar behavior in their investigation regarding cell bioactivity on a flat Ti surface compared to an anodized Ti surface.[64] A significant cell spreading and attachment was observed on the anodized surface compared to roughened ZrO_2. This is due to the larger surface area and nanoscale features of anodized samples providing biomechanical cues to the cells, thereby allowing strong adhesion compared to on the flat Ti.[60] Moreover, such nano-topographical features on the anodized surface causes higher biological cell plasticity triggering stem cell differentiation processes.[68] Comparing the cell orientation and attachment morphology between 10, 20 and 30 min anodized samples, no significant difference is observed. This may likely be due to the similar surface composition of anodized surface with nanotube walls composed of TiO_2 and $Ti(OH)_4$. Additionally, non-significant difference in cell attachment between the nanotubes with 15–30 nm diameter is also seen by Park *et al.*[70] They reported that nanotubes with diameters of 15–30 nm show

higher amount of fibronectin and vitronectin adsorption on the surface resulting in an integrin mediated cell binding.[70]

Fig. 7 shows the fluorescence imaging of the cells after 3 and 24 h of seeding on the samples. The cell cytoskeleton was probed by staining the actin filaments using ActinRed 555 Readyprobe and the nucleus was probed using NucBlue stain that binds to the DNA of the cells. After 3 h of cell seeding, ZrO_2 samples (Fig. 7a) show well-adhered cells though with rounded morphology that is likely due to the cells anchoring on all directions, which is also corroborated by the FESEM data (Fig. 6). However, on 10, 20 and 30 min anodized Ti–ZrO_2 samples (Fig. 7c, e and g), cells show elongated morphology likely due to the hydrophilic nanotubular features of the anodized surface. Huang *et al.* also observed superior cell spreading on the anodized Ti–6Al–4V samples due to larger filopodia extension.[71] They report that nanotubular features on the anodized surface interact with nano-scale cell membrane proteins (*i.e.*, integrin) promoting integrin clustering on the cell membrane, which allows cells to make focal adhesion with the substrates.[71] Cellular elongation is necessary for cell differentiation as mentioned above, through which the nucleus confirmation changes, which then transduces signals inside the nucleus to unfold the DNA and thereby triggers stem cell differentiation.[68] After 24 h of cell culturing, significant increase in cell number as well as spreading is observed on all the substrates as shown in Fig. 7b, d, f, and h. From fluorescence microscopy, it is observed that the anodized surface allows cells to spread and elongate at the early period (after 3 h) of incubation, whereas roughened ZrO_2 samples show elongated cell morphology only after 24 h of incubation. Such behavior of cells with well spreading and attachment observed on anodized surface may indicate its ability to provide bone-implant primary stability within 3 h as compared to 24 h. Fig. 8 shows the quantitative cell viability data of all the surfaces after 1 and 6 days of incubation. A significant ($p < 0.05$) increase in cells was observed on anodized Ti–ZrO_2 samples compared to roughened ZrO_2 after 6 days of incubation. No difference in cells was observed between 10TNZ and 20TTNZ samples either after 1 or 6 days of incubation. Likewise, no difference in cells was observed between 20TTNZ and 30TTNZ after 1 or 6 days of incubation. An increase in cells were observed from 1 to 6 days of incubation on all anodized Ti–ZrO_2 samples compared with no difference on roughened ZrO_2 sample from day 1 to day 6, which indicates that anodized Ti is biologically more active for enhancing cell response compared to the ZrO_2 surface. *In vivo* studies are required in future, where Ti–ZrO_2 samples with TiO_2 nanotubes are implanted inside rat femur, to investigate the rate of osseointegration.

Conclusion

ZrO_2 has been considered a potential alternative material for dental implants due to its tooth colored appearance. However, its bioactivity compared to titanium implants is still uncertain. Therefore, in this study the bioactivity of ZrO_2 *vs.* different topographies of titanium deposited ZrO_2 has been investigated. It was concluded that depositing titanium on ZrO_2 substrate improves the bioactivity of the ZrO_2 substrate in terms of enhanced cell viability, cell attachment and cell elongation. However, due to the gray colored appearance of Ti, the white colored appearance of ZrO_2 is compromised. Therefore, the formation of titania nanotubes for 20 and 30 min in 2 vol% H_2O, 0.25 wt% NH_4F in EG at 60 V on the ZrO_2 substrates was conducted. The achieved surface (TTNZ) improves cellular viability, cell adhesion, and cell elongation, and also maintains the white colored appearance of the ZrO_2 substrate. Such cellular behavior is known to occur due to the favorable surface characteristics and roughness of TNT surfaces which is composed of TiO_2 and $Ti(OH)_4$ and is characterized by a significantly high surface area. The aforementioned factors not only provide high surface area for cellular attachment but also higher surface hydrophilicity can allow fibronectin and vitronectin attachment with the nanotubular surface, which in turn leads to integrin mediated elongated cell attachment. Additionally, it is important to note that significant improvement on the cell spreading was observed on the anodized surface without having to anneal the surface, which provides the added benefit of avoiding the annealing step. Future direction of this work will be to investigate the hMSCs differentiation on anodized Ti–ZrO_2 substrates, to understand the mechanical stability of titania nanotubes on the ZrO_2 substrate, and to perform the *in vivo* investigation in order to study the osseointegration rate.

Acknowledgements

The authors would like to thank Maria Runa for the surface roughness measurements performed in Dr Wimmers' Tribology lab at Rush University Medical Center. This work made use of instrument in the Electron Microscopy Service (Research Resource Center, UIC). Financial support was provided by the Mechanical Engineering Department at MTU. We are grateful to National Science Foundation, DMR Grant # 1564950 and CBET Grant # 1067424, for making some of our characterizations possible.

References

1 H. M. Grandin, S. Berner and M. Dard, A Review of Titanium Zirconium (TiZr) Alloys for Use in Endosseous Dental Implants, *Materials*, 2012, **5**(12), 1348–1360.
2 Facts and Figures on Dental Implants, Dental Implants Facts and Figures 2014, cited 2014 August 28, http://www.aaid.com/about/press_room/dental_implants_faq.html.
3 M. Özcan and C. Hämmerle, Titanium as a Reconstruction and Implant Material in Dentistry: Advantages and Pitfalls, *Materials*, 2012, **5**(12), 1528–1545.
4 D. Hagi, *Biomechanical and Clinical Attributes of Zirconia Dental Implants – Two Case Reports*, Oral Health Group, 2013, cited 2014 6th October, http://www.oralhealthgroup.com/news/biomechanical-and-clinical-attributes-of-zirconia-dental-implants-two-case-reports/1002516574/?&er=NA.

5 D. Little, Zirconia: Conservative Options in Metal-Free Dentistry, *Dentsply Prosthetics*, 2006, 5.
6 A.-E. Borgonovo, A. Fabbri, V. Vavassori, R. Censi and C. Maiorana, Multiple teeth replacement with endosseous one-piece yttrium-stabilized zirconia dental implants, *Med. Oral Patol. Oral Cir. Bucal.*, 2012, **17**(6), 7.
7 S. M. Zahnmed and P. A. Assal, The Osseointegration of Zirconia Dental Implants, *Research and Science*, 2013, **123**, 12.
8 M. Goutam, G. Chandu, S. K. Mishra, M. Singh and B. Singh Tomar, Factors affecting Osseointegration: A Literature Review, *J. Orofacial Research*, 2013, **3**(3), 5.
9 C. Yao, E. B. Slamovich and T. J. Webster, Enhanced osteoblast functions on anodized titanium with nanotube-like structures, *J. Biomed. Mater. Res., Part A*, 2008, **85A**(1), 157–166.
10 M. Andreiotelli and R. J. Kohal, Fracture strength of zirconia implants after artificial aging, *Clin. Implant Dent. Relat. Res.*, 2009, **11**(2), 158–166.
11 R. J. Kohal, D. Weng, M. Bächle and J. R. Strub, Loaded custom-made zirconia and titanium implants show similar osseointegration: an animal experiment, *J. Periodontol.*, 2004, **75**(9), 1262–1268.
12 R. Depprich, H. Zipprich, M. Ommerborn, C. Naujoks, H. P. Wiesmann, S. Kiattavorncharoen, H. C. Lauer, U. Meyer, N. R. Kübler and J. Handschel, Osseointegration of zirconia implants compared with titanium: an *in vivo* study, *Head Face Med.*, 2008, **4**(1), 1–8.
13 M. Gahlert, S. Röhling, M. Wieland, C. M. Sprecher, H. Kniha and S. Milz, Osseointegration of zirconia and titanium dental implants: a histological and histomorphometrical study in the maxilla of pigs, *Clin. Oral Implants Res.*, 2009, **20**(11), 1247–1253.
14 M. Gahlert, T. Gudehus, S. Eichhorn, E. Steinhauser, H. Kniha and W. Erhardt, Biomechanical and histomorphometric comparison between zirconia implants with varying surface textures and a titanium implant in the maxilla of miniature pigs, *Clin. Oral Implants Res.*, 2007, **18**(5), 662–668.
15 S. Oh, C. Daraio, L. H. Chen, T. R. Pisanic, R. R. Fiñones and S. Jin, Significantly accelerated osteoblast cell growth on aligned TiO_2 nanotubes, *J. Biomed. Mater. Res., Part A*, 2006, **78A**(1), 97–103.
16 A. R. Elmore, Final report on the safety assessment of aluminum silicate, calcium silicate, magnesium aluminum silicate, magnesium silicate, magnesium trisilicate, sodium magnesium silicate, zirconium silicate, attapulgite, bentonite, Fuller's earth, hectorite, kaolin, lithium magnesium silicate, lithium magnesium sodium silicate, montmorillonite, pyrophyllite, and zeolite, *Int. J. Toxicol.*, 2003, **22**(1), 37–102.
17 C. J. Frandsen, K. Noh, K. S. Brammer, G. Johnston and S. Jin, Hybrid micro/nano-topography of a TiO_2 nanotube-coated commercial zirconia femoral knee implant promotes bone cell adhesion *in vitro*, *Mater. Sci. Eng., C*, 2013, **33**(5), 2752–2756.
18 J. C. Grotberg, Modifying Ti_6Al_4V Implant Surfaces: Cell Responses and Corrosion Resistance of Annealed Titania Nanotubes, in *Bioengineering*. 2014, University of Illinois at Chicago, p. 115.
19 S. B. Patel, A. Hamlekhan, D. Royhman, A. Butt, J. Yuan, T. Shokuhfar, C. Sukotjo, M. T. Mathew, G. Jursich and C. G. Takoudis, Enhancing surface characteristics of Ti–6Al–4V for bio-implants using integrated anodization and thermal oxidation, *J. Mater. Chem. B*, 2014, **2**(23), 3597–3608.
20 A. Hamlekhan, A. Butt, S. Patel, D. Royhman, C. Takoudis, C. Sukotjo, J. Yuan, G. Jursich, M. T. Mathew, W. Hendrickson, A. Virdi and T. Shokuhfar, Fabrication of Anti-Aging TiO_2 Nanotubes on Biomedical Ti Alloys, *PLoS One*, 2014, **9**(5), e96213.
21 D. H. Shin, T. Shokuhfar, C. Kyoung Choi, S.-H. Lee and C. Friedrich, Wettability changes of TiO_2 nanotube surfaces, *Nanotechnology*, 2011, **22**(31), 315704.
22 D. M. Rivera-Chacon, M. Alvarado-Velez, C. Y. Acevedo-Morantes, S. P. Singh, E. Gultepe, D. Nagesha, S. Sridhar and J. E. Ramirez-Vick, Fibronectin and vitronectin promote human fetal osteoblast cell attachment and proliferation on nanoporous titanium surfaces, *J. Biomed. Nanotechnol.*, 2013, **9**(6), 1092.
23 X. Zhu, J. Chen, L. Scheideler, R. Reichl and J. Geis-Gerstorfer, Effects of topography and composition of titanium surface oxides on osteoblast responses, *Biomaterials*, 2004, **25**(18), 4087–4103.
24 C. Strobel, N. Bormann, A. Kadow-Romacker, G. Schmidmaier and B. Wildemann, Sequential release kinetics of two (gentamicin and BMP-2) or three (gentamicin, IGF-I and BMP-2) substances from a one-component polymeric coating on implants, *J. Controlled Release*, 2011, **156**(1), 37–45.
25 B. G. X. Zhang, D. E. Myers, G. G. Wallace, M. Brandt and P. F. Choong, Bioactive Coatings for Orthopaedic Implants—Recent Trends in Development of Implant Coatings, *Int. J. Mol. Sci.*, 2014, **15**(7), 11878–11921.
26 J. Park, S. Bauer, A. Pittrof, M. S. Killian, P. Schmuki and K. von der Mark, Synergistic Control of Mesenchymal Stem Cell Differentiation by Nanoscale Surface Geometry and Immobilized Growth Factors on TiO_2 Nanotubes, *Small*, 2012, **8**(1), 98–107.
27 K. C. Popat, M. Eltgroth, T. J. LaTempa, C. A. Grimes and T. A. Desai, Titania Nanotubes: A Novel Platform for Drug-Eluting Coatings for Medical Implants?, *Small*, 2007, **3**(11), 1878–1881.
28 T. Shokuhfar, S. Sinha-Ray, C. Sukotjo and A. L. Yarin, Intercalation of anti-inflammatory drug molecules within TiO_2 nanotubes, *RSC Adv.*, 2013, **3**(38), 17380–17386.
29 M. S. Aw, K. Khalid, K. Gulati, G. J. Atkins, P. Pivonka, D. M. Findlay and D. Losic, Characterization of drug-release kinetics in trabecular bone from titania nanotube implants, *Int. J. Nanomed.*, 2012, **7**, 10.
30 D. Regonini, C. R. Bowen, A. Jaroenworaluck and R. Stevens, A review of growth mechanism, structure and crystallinity of anodized TiO_2 nanotubes, *Mater. Sci. Eng., R*, 2013, **74**(12), 377–406.

31 C. A. Grimes and G. K. Mor, *TiO_2 nanotube array*, Springer Science+Business Media, New York, 2009, p. 380.
32 H. Yin, H. Liu and W. Z. Shen, The large diameter and fast growth of self-organized TiO_2 nanotube arrays achieved *via* electrochemical anodization, *Nanotechnology*, 2010, **21**, 8.
33 S. Berger, P. Roy and P. Schmuki, TiO_2 Nanotubes: Synthesis and Applications, *Angew. Chem., Int. Ed.*, 2011, **50**, 36.
34 B. Chen, J. Hou and K. Lu, Formation Mechanism of TiO_2 Nanotubes and Their Applications in Photoelectrochemical Water Splitting and Supercapacitors, *Langmuir*, 2013, **29**(19), 5911–5919.
35 K. R. Hebert, S. P. Albu, I. Paramasivam and P. Schmuki, Morphological instability leading to formation of porous anodic oxide films, *Nat. Mater.*, 2011, **11**(2), 162–166.
36 S. J. Garcia-Vergara, P. Skeldon, G. E. Thompson and H. Habazaki, A flow model of porous anodic film growth on aluminium, *Electrochim. Acta*, 2006, **52**(2), 681–687.
37 P. Skeldon, G. E. Thompson, S. J. Garcia-Vergara, L. Iglesias-Rubianes and C. E. Blanco-Pinzon, A Tracer Study of Porous Anodic Alumina, *Electrochem. Solid-State Lett.*, 2006, **9**(11), 5.
38 A. Z. Sadek, H. Zheng, K. Latham, W. Wlodarski and K. Kalantar-Zadeh, Anodization of Ti Thin Film Deposited on ITO, *Langmuir*, 2009, **25**(1), 509–514.
39 T. Yu-Xin, T. Jie, Z. Yan-Yan, W. Tao, T. Hai-Jun and Z. Ya-Rong, Preparation of TiO_2 nanotube on glass by anodization of Ti films at room temperature, *Trans. Nonferrous Met. Soc. China*, 2009, **19**, 7.
40 J. Tupala, M. Kemell, E. Härkönen, M. Ritala and M. Leskelä, Preparation of regularly structured nanotubular TiO_2 thin films on ITO and their modification with thin ALD-grown layers, *Nanotechnology*, 2012, **23**(12), 125707.
41 D. W. Liu, C. H. Perry and R. P. Ingel, Infrared spectra in nonstoichiometric yttria-stabilized zirconia mixed crystals at elevated temperatures, *J. Appl. Phys.*, 1988, **64**(3), 1413–1417.
42 H. L. Ningyuan Duan, L. Li, J. Hu, L. Bi, H. Lu, X. Weng, J. Xie and L. Deng, ZrO_2-TiO_2 thin films: a new material system for mid-infrared integrated photonics, *Opt. Mater. Express*, 2013, **3**(9), 9.
43 J. Judes and V. Kamaraj, Preparation and characterization of yttria stabilized zirconia minispheres by the sol–gel drop generation method, *Mater. Sci.*, 2009, **27**(2), 9.
44 P. Ganesh babu, C. Kumar, K. Ravichandran and P. Manohar, Synthesis and Characterization of Zirconium Tin Titanate ($Zr_{0.8}Sn_{0.2}TiO_4$), *Int. J. ChemTech Res.*, 2013, **5**(5), 8.
45 S. K. Sharma and S. Som, Eu^{3+}/Tb^{3+}-codoped Y_2O_3 nanophosphors: Rietveld refinement, bandgap and photoluminescence optimization, *J. Phys. D: Appl. Phys.*, 2012, **45**(415102), 12.
46 E.-M. Köck, M. Kogler, T. Bielz, B. Klötzer and S. Penner, *In Situ* FT-IR Spectroscopic Study of CO_2 and CO Adsorption on Y_2O_3, ZrO_2, and Yttria-Stabilized ZrO_2, *J. Phys. Chem. C*, 2013, **117**(34), 17666–17673.
47 M.-C. Rosu, R.-C. Suciu, M. Mihet and I. Bratu, Physical–chemical characterization of titanium dioxide layers sensitized with the natural dyes carmine and morin, *Mater. Sci. Semicond. Process.*, 2013, **16**(6), 1551–1557.
48 T. Bezrodna, G. Puchkovska, V. Shymanovska, J. Baran and H. Ratajczak, IR-analysis of H-bonded H_2O on the pure TiO_2 surface, *J. Mol. Struct.*, 2004, **700**(1–3), 175–181.
49 D. C. L. Vasconcelos, Infrared Spectroscopy of Titania Sol–Gel Coatings on 316L Stainless Steel, *Mater. Sci. Appl.*, 2011, **02**(10), 1375–1382.
50 D. Velten, V. Biehl, F. Aubertin, B. Valeske, W. Possart and J. Breme, Preparation of TiO_2 layers on cp-Ti and Ti_6Al_4V by thermal and anodic oxidation and by sol–gel coating techniques and their characterization, *J. Biomed. Mater. Res.*, 2002, **59**(1), 18–28.
51 V. A. Zeitler and C. A. Brown, The Infrared Spectra of Some Ti–O–Si, Ti–O–Ti and Si–O–Si Compounds, *J. Phys. Chem.*, 1957, **61**(9), 1174–1177.
52 R.-J. Wu, Y.-L. Sun, C.-C. Lin, H.-W. Chen and M. Chavali, Composite of TiO_2 nanowires and Nafion as humidity sensor material, *Sens. Actuators, B*, 2006, **115**(1), 198–204.
53 K. Hadjiivanov, J. Lamotte and J.-C. Lavalley, FTIR Study of Low-Temperature CO Adsorption on Pure and Ammonia-Precovered TiO_2 (Anatase), *Langmuir*, 1997, **13**(13), 3374–3381.
54 H. U. Lee, S. C. Lee, S. Choi, B. Son, S. M. Lee, H. J. Kim and J. Lee, Efficient visible-light induced photocatalysis on nanoporous nitrogen-doped titanium dioxide catalysts, *Chem. Eng. J.*, 2013, **228**, 756–764.
55 G. Zhao, Z. Schwartz, M. Wieland, F. Rupp, J. Geis-Gerstorfer, D. L. Cochran and B. D. Boyan, High surface energy enhances cell response to titanium substrate microstructure, *J. Biomed. Mater. Res., Part A*, 2005, **74A**(1), 49–58.
56 A. B. Novales Jr, S. L. de Souza, R. R. Martins de Barros, K. K. Yamashina Pereira, G. Iezzi and A. Piattelli, In fluence of Implant Surfaces on Osseointegration, *Braz. Dent. J.*, 2010, **21**(6), 11.
57 J. H. Park, C. E. Wasilewski, N. Almodovar, R. Olivares-Navarrete, B. D. Boyan, R. Tannenbaum and Z. Schwartz, The responses to surface wettability gradients induced by chitosan nanofilms on microtextured titanium mediated by specific integrin receptors, *Biomaterials*, 2012, **33**(30), 7386–7393.
58 M. L. González-Martín, L. Labajos-Broncano, B. Jańczuk and J. M. Bruque, Wettability and surface free energy of zirconia ceramics and their constituents, *J. Mater. Sci.*, 1999, **34**(23), 5923–5926.
59 A. Noro, M. Kaneko, I. Murata and M. Yoshinari, Influence of surface topography and surface physicochemistry on wettability of zirconia (tetragonal zirconia polycrystal), *J. Biomed. Mater. Res., Part B*, 2013, **101B**(2), 355–363.
60 M. Taborelli, M. Jobin, P. François, P. Vaudaux, M. Tonetti, S. Szmukler-Moncler, J. P. Simpson and P. Descouts, Influence of surface treatments developed for oral implants on the physical and biological properties of titanium. (I) Surface characterization, *Clin. Oral Implants Res.*, 1997, **8**(3), 208–216.

61 F. Rupp, L. Scheideler, N. Olshanska, M. de Wild, M. Wieland and J. Geis-Gerstorfer, Enhancing surface free energy and hydrophilicity through chemical modification of microstructured titanium implant surfaces, *J. Biomed. Mater. Res., Part A*, 2006, **76A**(2), 323–334.

62 K. J. Kubiak, M. C. T. Wilson, T. G. Mathia and P. H. Carval, Wettability *versus* roughness of engineering surfaces, *Wear*, 2011, **271**(3–4), 523–528.

63 N. B. Dahotre, S. R. Paital, A. N. Samant and C. Daniel, *Wetting behaviour of laser synthetic surface microtextures on Ti–6Al–4V for bioapplication*, 2010, vol. 368, pp. 1863–1889.

64 K. C. Popat, L. Leoni, C. A. Grimes and T. A. Desai, Influence of engineered titania nanotubular surfaces on bone cells, *Biomaterials*, 2007, **28**(21), 3188–3197.

65 N. Wang, H. Li, W. Lü, J. Li, J. Wang, Z. Zhang and Y. Liu, Effects of TiO_2 nanotubes with different diameters on gene expression and osseointegration of implants in minipigs, *Biomaterials*, 2011, **32**(29), 6900–6911.

66 A. F. Mavrogenis, R. Dimitriou, J. Parvizi and G. C. Babis, Biology of Implant Osseointegration, *J. Musculoskeletal Neuronal Interact.*, 2009, **9**(2), 11.

67 T. Shokuhfar, A. Hamlekhan, J. Y. Chang, C. K. Choi, C. Sukotjo and C. Friedrich, Biophysical evaluation of cells on nanotubular surfaces: the effects of atomic ordering and chemistry, *Int. J. Nanomed.*, 2014, **9**, 3737–3748.

68 S. Oh, K. S. Brammer, Y. S. Julie Li, D. Teng, A. J. Engler, S. Chien and S. Jin, Stem cell fate dictated solely by altered nanotube dimension, *Proc. Natl. Acad. Sci. U. S. A.*, 2009, **106**(7), 2130–2135.

69 A. Pae, H. Lee, H. S. Kim, Y. D. Kwon and Y. H. Woo, Attachment and growth behaviour of human gingival fibroblasts on titanium and zirconia ceramic surfaces, *Biomed. Mater.*, 2009, **4**(2), 025005.

70 J. Park, S. Bauer, K. von der Mark and P. Schmuki, Nanosize and Vitality: TiO_2 Nanotube Diameter Directs Cell Fate, *Nano Lett.*, 2007, **7**(6), 1686–1691.

71 H.-H. Huang, C.-P. Wu, Y.-S. Sun, W.-E. Yang and T.-H. Lee, Surface nanotopography of an anodized Ti–6Al–7Nb alloy enhances cell growth, *J. Alloys Compd.*, 2014, **615**, S648–S654.

